Available online at www.sciencedirect.com
SCIENCE DIRECT®
Mechanics of Materials 35 (2003) 53–68
MECHANICS OF MATERIALS
www.elsevier.com/locate/mechmat

On the effective lattice parameter of binary alloys

V.A. Lubarda *

Department of Mechanical and Aerospace Engineering Sciences, University of California, 9500 Gilman Drive, San Diego, La Jolla, CA 92093-0411, USA

Received 24 May 2002

Dedicated to the memory of Dr. Owen Richmond

Abstract

A study of the effective lattice parameter in binary alloys is given based on an analysis of the volume change produced by dilute resolution of the solute atoms in the solvent matrix. An apparent size of the solute atom is incorporated in the analysis to approximately account for the electronic interactions between the outermost quantum shells of the solute and solvent atoms. The comparison with experimental data for various alloy systems and deviations from Vegard's law are analyzed. The free energy of binary alloys and the ordering of solute atoms at higher solute concentrations are then discussed.
© 2002 Elsevier Science Ltd. All rights reserved.

Keywords: Binary alloys; Lattice parameter; Vegard's law; Solute atoms; Apparent atomic radius; Nonlinear elasticity; Free energy

1. Introduction

In the vicinity of each solute atom which is resolved in a solvent matrix there is a considerable variation of interatomic spacing due to local distortions of the crystalline structure. Away from the solute, the atoms occupy positions of an ideal, regular lattice whose spacing represents an average spacing over several thousand atomic distances. The X-ray diffraction lines from a solid solution are thus almost as sharp as from pure metal, and occur at angles corresponding to this average lattice spacing. The lattice spacing is a fundamental quantity related to bulk properties of the solid solution, such as elastic coefficients, thermal expansion, chemical bonding, and electrical conductivity, as well as to the onset of phase transition, occurrence of stacking faults, dislocation nucleation, etc. Analytical determination of the effective lattice parameter in terms of the properties of the constituting elements of the solution has been a long-standing research topic in the solid state physics and materials science. Vegard (1921) observed that in the cases when two salts form a continuous solid solution, the effective lattice parameter often varies almost linearly with the solute concentration, as a weighted mean of the lattice spacings of the solute and solvent. This empirical rule has become known as Vegard's law, although subsequent experimental and theoretical investigations have shown that very few other, particularly metallic, solid solutions have lattice spacings

* Tel.: +1-858-534-3169; fax: +1-858-534-5698.
E-mail address: vlubarda@ucsd.edu (V.A. Lubarda).

0167-6636/03/$ - see front matter © 2002 Elsevier Science Ltd. All rights reserved.
PII: S0167-6636(02)00196-5

which agree with a linear relationship between the two end points of alloying elements. Nevertheless, when studying solid solutions, it became a common practice to speak about deviations or departures from Vegard's law (e.g., Hume-Rothery et al., 1969).

Among the factors that affect the structure and formation of an alloy, the prominent include the difference in atomic size, the electro-chemical properties of the alloying elements, and their crystalline structures. The size effect has been often studied from an idealized point of view by methods of continuum elasticity. A solid spherical inclusion inserted into a spherical hole of a matrix material was considered to be a model of substitutional or interstitial atom. The size disparity between the solute and solvent atoms causes the volume change of the solution, and this can be related to the effective lattice parameter. Linear elasticity was most frequently employed (Pines, 1940; Seitz, 1946; Lawson, 1947; Friedel, 1954, 1955; Eshelby, 1954, 1956), although nonlinear effects were also considered (Gschneidner and Vineyard, 1962; Park et al., 1975; Lubarda and Richmond, 1999). For certain alloy systems this has led to satisfactory agreement with experimental results, but in many cases the predicted lattice spacing was significantly above or below the measured values. King (1966) indicated that in alloys where the solute atom is smaller than the solvent atom, the sign of the predicted change in atomic volume was always found to be in error. Where the atomic volume of solute is greater, the predicted and observed values agreed to within 5% in only half of the considered random selection of alloy systems. The results for many solutions based on iron, copper, aluminum, and magnesium were poor. For Au–Ag alloy, the analysis predicted an increase of the effective lattice parameter due to substitution of larger silver atom in the solvent matrix of smaller gold atoms. The measurements, however, indicate a decrease of the effective lattice parameter (Pearson, 1972). Similar situation was found with many other systems; the lattice distortion of the nickel lattice with germanium as the solute is opposite in sense than expected from the relative sizes of the elemental atoms (Chessin et al., 1963).

The reason for a limited success of continuum elasticity models is not surprising, since in view of its atomistic scale the problem is fundamentally one of the quantum-mechanics and physical chemistry. The electronic interactions between the outer-most quantum shells of the solute and solvent atoms depend on their electro-chemical characteristics, partially reflected by their positions in the periodic table of elements, and are far too complex to be accounted for only by a simple size factor. For example, the alloy systems whose two end members have similar, if not identical, outer electronic structures, show better agreement with predictions based on elasticity models and Vegard's law. King (1966) suggested that a tendency of metallic solid solution to deviate from Vegard's law may actually be taken as a measure of the modification of the electronic environment of the solute atom. At higher concentrations, sufficient amount of solute has been added to modify the electronic environment of solvent atoms, as well. Sarkisov (1960) proposed an electron-gas model to explain these deviations, while Steinwehr (1967) combined purely geometrical and chemical interaction effects, closely related to the difference in electronegativities of the solute and solvent atoms. Yet, none of these models was able to predict the effective lattice parameter with a satisfactory accuracy for a large number of randomly selected binary alloy combinations.

There has been a significant amount of research devoted to theoretical and experimental determination of the effective lattice parameter in more complex alloy systems. An accurate X-ray diffraction measurement of the lattice parameter of a ternary $Cu_{99-x}Au_xFe_1$ alloy along the gold concentration range was reported by Finkler et al. (1987). A positive deviation from the linearity of Vegard's law was observed. Similar observations were reported for ternary layered intercalation compounds by Solin et al. (1989). The applicability of Vegard's rule in complicated oxides with spinel and perovskite structures was also studied (e.g., Talanov, 1983; Yashima et al., 1992; Ganguly et al., 1993). Nongkynrih et al. (1988) observed two different types of linear behavior in the regions below and above the mid-point of the concentration range of the substitute in calcium and lead

based apatits, which is a rather general property, since in most systems the linear trends at the two limiting ends of the concentration range are quite different. A geometric model suggested by Urusov (1992) involves the calculation of the atomic displacement around substitutional atoms at the level of the first and second nearest neighbors.

In this paper we derive an expression for the effective lattice parameter of binary solid solutions by using an elasticity inclusion model, in conjunction with an apparent size of the solute atom when resolved in the solvent matrix. The latter is intended to approximately account for the electronic interactions between the outermost quantum shells of the solute and solvent atoms. The comparison with experimental results for various alloy systems and deviations from Vegard's law are considered. The free energy of binary alloys and the ordering of solute atoms at higher solute concentrations are then discussed.

2. Volume change due to solute atom

Consider a solvent material of volume V enclosed by the surface S, free of any external load or surface constraint. Remove a solvent atom, imagined to be a small sphere of radius R_1 deep inside the volume V, and replace it by a solute atom of radius $R_2 > R_1$ (an analogous derivation proceeds in the case $R_2 < R_1$). It will be assumed that the solute atom is a spherical inclusion whose elastic properties are equal to those of the solute material in bulk. The external surface S expands, causing an increase ΔV of the volume within S. As in Eshelby (1954, 1956), this volume increase can be calculated in two steps. First, the solute atom is considered to be inserted in an infinite medium of the solvent matrix. The points on an imagined internal surface, having the size and shape of S, are far from the solute atom and, thus, neglecting local crystal anisotropy, have displacements governed by

$$u_1^\infty(r) = C\frac{R_1^3}{r^2}, \tag{1}$$

where (Lubarda and Richmond, 1999)

$$C = \frac{1}{\gamma_2}\left[\frac{\Delta}{R_1} + c\left(\frac{\Delta}{R_1}\right)^2\right] \tag{2}$$

and

$$\gamma_2^2 c = \frac{3\mu_1 + n_1}{3\kappa_2} - 1 - \left(\frac{9l_2 + n_2}{3\kappa_2} + \frac{1}{2}\right)(\gamma_2 - 1)^2 - \frac{\gamma_2}{\gamma_1}\frac{\mu_1 + 2m_1}{\kappa_1}. \tag{3}$$

The parameters γ_1 and γ_2 are defined by

$$\gamma_1 = 1 + \frac{4\mu_1}{3\kappa_1}, \quad \gamma_2 = 1 + \frac{4\mu_1}{3\kappa_2}. \tag{4}$$

The third-order elastic moduli of the solute material are l_1, m_1, and n_1 (Murnaghan, 1951; Toupin and Bernstein, 1961). In the case of small misfit and linear elasticity, the constant C in Eq. (2) reduces to

$$C = \frac{1}{\gamma_2}\frac{\Delta}{R_1}. \tag{5}$$

The volume increase within S is, therefore,

$$\Delta V^\infty = \int_S \mathbf{u}_1^\infty \cdot \mathbf{n}\,\mathrm{d}S = 4\pi R_1^3 C, \tag{6}$$

where $\mathbf{n}$ is the outward normal to S. This follows by the Gauss divergence theorem, recalling that for any m and the three-dimensional vector $\mathbf{r}$, $\mathrm{div}(r^m\mathbf{r}) = (m+3)r^m$.

An auxiliary problem is next considered with the image traction $\mathbf{t}^{\mathrm{im}} = -\mathbf{n}\cdot\sigma_1^\infty$ applied over the external surface S of the finite body V with the inserted inclusion. The superposition of two problems makes the total traction over the surface S equal to zero, and hence represents the solution of the original problem. Since the inclusion is small comparing to volume V, in the image problem we can neglect the fact that the material of the inclusion is different from the surrounding matrix. Consequently, the volume change in the image problem is

$$\Delta V^{\mathrm{im}} = \frac{1}{3\kappa_1}\int_S \mathbf{r}\cdot\mathbf{t}^{\mathrm{im}}\,\mathrm{d}S = \frac{4\mu_1}{3\kappa_1}\Delta V^\infty. \tag{7}$$

The last step follows from the relationship $\sigma_1^\infty = 2\mu_1\epsilon_1^\infty$, since ϵ_1^∞ is a traceless tensor, and because the displacement $u_1^\infty(r)$ is a homogeneous function

of degree −2. Therefore, upon summation of Eqs. (6) and (7), the volume increase produced by insertion of the solute atom is

$$\Delta V = 4\pi R_1^3 \gamma_1 C \tag{8}$$

with C given by Eq. (2). If C is given by Eq. (5), implying a small misfit and linear elasticity, Eq. (8) reduces to Eshelby's expression $\Delta V = V_{\text{mis}}\gamma_1/\gamma_2$, where $V_{\text{mis}} = 4\pi R_1^2 \Delta$ is the misfit volume. In this case $\Delta V^{\infty} = V_{\text{mis}}/\gamma_2$ and $\Delta V^{\text{im}} = (\gamma_1 - 1)V_{\text{mis}}/\gamma_2$.

The volume change can also be derived in a manner analogous to that used by Pines (1940). Consider a volume V_0 bounded by a traction free external surface S and the surface of a small hole of radius R_1 under the pressure p, deep inside the surface S. As an auxiliary problem consider the same body under hydrostatic pressure p over the external surface and the surface of the hole. By the Betti reciprocal theorem, the volume change ΔV_0 is $4\pi R_1^3 p/3\kappa_1$. The change of the volume V bounded by S (including the volume of the hole), produced by pressure p on the surface of the hole, is $\Delta V = \Delta V_0 + 4\pi R_1^2 u_0$, where u_0 is the displacement of the points on the surface of the hole. If the solid sphere of radius $R_1 + \Delta$ is to be inserted in the hole of radius R_1, the misfitting condition is $u_0 + pR_1/\ 3\kappa_2 = \Delta$, and therefore

$$\Delta V = 4\pi R_1^2 \Delta + \frac{4}{3} R_1^3 \pi \left(\frac{1}{\kappa_1} - \frac{1}{\kappa_2} \right) p. \tag{9}$$

Since the pressure required for insertion of a solid sphere into a small hole is given by $p = (4\mu_1/\gamma_2)\Delta/R_1$, the substitution into Eq. (9) again leads to Eq. (8), with C given by Eq. (5).

Yet another derivation of the expression for the volume change ΔV in the case of linear elasticity was constructed by Friedel (1955), who employed the elasticity theorem that the volume of a homogeneous medium does not alter upon introduction of an internal self-equilibrating state of stress. Thus, imagine that in place of the solute atom with the bulk modulus κ_2 and the radius R_2, we insert a fictitious solute atom with the bulk modulus κ_1 of the solvent matrix and with the radius R_2' adjusted so that the fictitious solute atom has the same radius R when inserted into the solvent matrix as does the original solute atom. Then, we have

$$\begin{aligned} R &= \left(1 - \frac{1}{\gamma_2}\right) R_1 + \frac{1}{\gamma_2} R_2 \\ &= \left(1 - \frac{1}{\gamma_1}\right) R_1 + \frac{1}{\gamma_1} R_2', \end{aligned} \tag{10}$$

where from $R_2' = R_1 + \gamma_1 \Delta/A$. The fictitious misfit is thus $\Delta' = R_2' - R_1 = \gamma_1 \Delta/\gamma_2$, and from the cited theorem $\Delta V = V_{\text{mis}}' = 4\pi R_1^2 \Delta' = \gamma_1 V_{\text{mis}}/\gamma_2$.

If $\kappa_1 = \kappa_2$, the volume change ΔV is equal to the misfit volume $4\pi R_1^2 \Delta$. Hence, in this case the increase of the volume of the matrix material is exactly balanced by the decrease in the volume of the inclusion (within linear elasticity model). The actual volume of the material does alter if the second-order elasticity effects are included in the analysis, as originally shown by Zener (1942) and verified by Seeger and Mann (1959). Gschneidner and Vineyard (1962) used Zener's formula in their second-order elasticity analysis of the Vegard's rule in binary alloys.

3. Volume change of a solid solution

To calculate the volume change associated with a random resolution of xN_1 solute atoms in the solvent matrix, imagine that solute atoms are first inserted into an infinite matrix. Since nonlinear elasticity effects are localized to regions around each solute atom, and assuming that these do not overlap (dilute distribution), we can calculate the volume change ΔV^{∞} of the material within the surface S by superposition as

$$\Delta V^{\infty} = xN_1 4\pi R_1^3 C. \tag{11}$$

The image traction $\mathbf{t}^{\text{im}} = -2\mu_1 \mathbf{n} \cdot \epsilon_1^{\infty}$ is then applied over the external surface S, associated with the displacement field $\mathbf{u}_1^{\infty} = R_1^3 C \mathbf{r}/r^3$ due to each inserted solute atom. Since the medium within the surface S is now a heterogeneous medium, composed of the solvent matrix and inserted solute atoms of concentration x, the effective shear and bulk moduli (μ and κ) can be calculated by using the Hill's self-consistent method (Nemat-Nasser and Hori, 1999). This gives

$$\begin{aligned} &\frac{1-x}{1 + 4\mu/3\kappa_1} + \frac{x}{1 + 4\mu/3\kappa_2} \\ &\quad - 5\left(\frac{1-x}{1 - \mu/\mu_2} + \frac{x}{1 - \mu/\mu_1} \right) + 2 = 0, \end{aligned} \tag{12}$$

$$\kappa = \left(\frac{1-x}{\kappa_1 + 4\mu/3} + \frac{x}{\kappa_2 + 4\mu/3} \right)^{-1} - \frac{4}{3}\mu. \tag{13}$$

The volume change in the image problem is accordingly

$$\Delta V^{\text{im}} = \frac{4\mu_1}{3\kappa} \Delta V^{\infty}. \tag{14}$$

Upon summation of Eqs. (11) and (14), the total volume change produced by insertion of the solute atoms is

$$\Delta V = xN_1 4\pi R_1^3 \gamma C, \quad \gamma = 1 + \frac{4\mu_1}{3\kappa}. \tag{15}$$

If the solute atom is only slightly larger than the matrix atom, linear elasticity applies and the volume change becomes

$$\Delta V = xN_1 \frac{\gamma}{\gamma_2} V_{\text{mis}}. \tag{16}$$

When the effective bulk modulus κ of the solution is replaced by the bulk modulus κ_1 of the solvent itself, Eq. (16) reduces to the Eshelby's (1956) result for dilute solutions and low concentration of solute atoms. The use of the effective bulk modulus accounts, to a certain extent, for elastic interactions among solute atoms in the case of more concentrated solutions.

4. Effective lattice parameter of binary alloys

In the vicinity of each solute atom, the atoms are not located at regular points of the ideal lattice. On proceeding outwards, local distortions disappear and atoms take positions of an ideal, uniformly expanded or contracted lattice. The Brag reflections from a solid solution are thus almost as sharp as those from a pure metal, and occur at angles corresponding to the lattice spacing averaged over approximately several thousand atomic distances. If the solvent material contains N_1 atoms of atomic volume Ω_1, its volume is $V = N_1\Omega_1$. When xN_1 randomly selected solvent atoms are replaced by solute atoms of atomic volume Ω_2, the volume V changes by ΔV. The effective atomic volume Ω of the resulting solid solution can be defined by $V + \Delta V = N_1\Omega$. This gives

$$\Omega = \Omega_1 + \frac{\Delta V}{N_1}. \tag{17}$$

Substituting Eq. (15) into Eq. (17), there follows

$$\Omega = \Omega_1 + 4\pi R_1^3 x \gamma C, \tag{18}$$

where x is the atomic concentration of solute. The radius of an atom is defined as the Seitz radius, which is related to the atomic volume by $\Omega = 4\pi R_1^3/3$. For example, assuming the small misfit,

$$4\pi R_1^3 \gamma_2 C = \Omega_2 - \Omega_1 \tag{19}$$

and Eq. (18) becomes

$$\Omega = \left(1 - \frac{\gamma}{\gamma_2} x\right)\Omega_1 + \frac{\gamma}{\gamma_2} x\Omega_2. \tag{20}$$

For $\gamma = \gamma_2$ this is the Zen's (1956) mixture rule of additive atomic (or molar) volumes of the solute and solvent.

If there are k atoms per unit lattice cell, the atomic volume is $\Omega = \vartheta a^3/k$, where a denotes the lattice parameter, and k equals to 1 for the simple cubic, 2 for the body-centered cubic, 4 for the face-centered cubic, 6 for the hexagonal close-packed, and 8 for the diamond-cubic lattice structure. For complex cubics, k takes larger values (e.g., $k = 58$ for the α-manganese). Furthermore, the parameter $\vartheta = 1$ for cubic lattices, and $\vartheta = 3\sqrt{3}c/2a \approx 4.2427$ for an ideal hexagonal close-packed lattice. Therefore, from Eq. (18) the effective lattice parameter of a binary alloy is

$$a = \left[a_1^3 + 4\pi R_1^3 x \frac{k_1}{\vartheta_1} \gamma C \right]^{1/3}. \tag{21}$$

In Eq. (21) it is assumed that the solution and solvent share the same lattice structures. If the solution has a different lattice structure, the right-hand side of Eq. (21) should be multiplied by $(k\vartheta_1/k_1\vartheta)^{1/3}$. Since the Seitz radius of an atom is related to the lattice parameter by $R = (3\vartheta/4\pi k)^{1/3} a$, from Eq. (2) it follows that $C = C(a_1, a_2)$ in Eq. (21).

5. Apparent radius of the solute atom

The following stipulation regarding the size of the solute atom will be implemented in the subsequent analysis. If the radius of the solute atom in

its parent lattice is R_2, the radius of the solute atom, when inserted into the solvent matrix, will partially change without any mechanical action by the transfer of electrons between high-energy quantum shells of the solute and solvent atoms. This is due to the fact that the outer electron clouds of atoms in a crystalline structure are more or less diffused than those in the free atomic state, or those in a different atomic environment. The often large differences between atomic and ionic radii of elements would be an extreme illustration of this effect. This will be incorporated in the elasticity analysis by assuming that a solute atom of an apparent radius $R_2^* = \eta_2 R_2$ is substituted in place of the solvent atom of radius R_1. The pressure is only required to bridge the apparent misfit between the solute and solvent atom, $\Delta^* = R_2^* - R_1$, during which the inner electron shells (inert-gas core) of the solute atom deforms, as well. The coefficient η_2 can be slightly greater or smaller than one. Its value depends on the atomic structures, relative valence and electronegativity difference between the solute and solvent (bond energy), ratio of the number of valence electrons to the number of atoms in the unit cell (electron concentration), the coordination number, and the crystalline structure of the solvent. In principle, this could be determined or estimated by the quantum mechanics or physical chemistry considerations (Pauling, 1956, 1960; Mott, 1962; Blandin, 1965; Weiss, 1990), which is beyond the scope of this paper. For example, the parameter η_2 should be more nearly equal to one, more similar are the outer electron structures of the solute and solvent.

The apparent atomic radius of the solute atom considered here is analogous to the apparent atomic radius used by Axon and Hume-Rothery (1948). They calculated the apparent radius (based on the closest distance definition) from the apparent lattice spacing of the solute, which was obtained by extrapolating the initial linear lattice spacing vs. composition variation at small concentration of solute to 100 at.% of solute. The same idea was used by Massalski and King (1961), and King (1965, 1966), who defined the effective atomic volume of the solute by linear extrapolation of the initial volume plot to 100% solute. They observed that at low values of the solute concentration the atomic volumes of solid solutions vary linearly with composition. In many systems this linear trend continues up to the phase boundary; in other systems there is a limiting concentration above which the volume change is no longer linear.

The electronic interactions between the solute and solvent atoms also affect the compressibility of the solute atom. We could then assume that the elastic bulk modulus of the solute in solvent environment is different from that of the solute in its pure state. The consequences of this modification would not be particularly significant for the calculation of the strain energy of an alloy (at low concentration of solute), since this is dominantly stored in the solvent matrix, but it could be important for the calculation of effective properties of an alloy. For example, the building up of 3d electron shells, which may occur in the solute atoms of transition elements during alloying process, can suddenly increase the compressibility of the atom by an increased atomic cohesion.

6. Deviations from Vegard's law

The effect of the parameter η_2 will be included in the sequel by replacing the radius of the solute atom R_2 in all previous expressions by $\eta_2 R_2$. The apparent misfit to be bridged during the insertion process is

$$\Delta^* = \eta_2 R_2 - R_1. \tag{22}$$

If only linear term in the misfit is retained in the expression for C, the effective lattice parameter becomes

$$a = \left[a_1^3 + 3x\frac{\gamma}{\gamma_2}a_1^2(\zeta a_2 - a_1)\right]^{1/3},$$
$$\frac{\gamma}{\gamma_2} = \frac{1 + 4\mu_1/3\kappa}{1 + 4\mu_1/3\kappa_2}, \tag{23}$$

where

$$\zeta = \eta_2 \sqrt[3]{\frac{\vartheta_2 k_1}{\vartheta_1 k_2}}. \tag{24}$$

By further straightforward approximation, the lattice parameter becomes

$$a = \left(1 - \frac{\gamma}{\gamma_2}x\right)a_1 + \left(\zeta\frac{\gamma}{\gamma_2}x\right)a_2. \tag{25}$$

If the solute atoms are much more compressible than the solvent matrix, γ/γ_2 is small and the lattice parameter of the solution is nearly equal to the lattice parameter of the solvent ($a \approx a_1$).

Terminal solid solution at the other end of the phase diagram can be considered by reversing the roles of two materials. Thus, Eq. (21) is replaced with

$$a = \left[a_2^3 + 4\pi R_2^3(1-x)\frac{k_2}{\vartheta_2}\gamma C\right]^{1/3}, \quad \gamma = 1 + \frac{4\mu_2}{3\kappa}. \tag{26}$$

The parameter C is again defined by Eq. (2), in which the indices 1 and 2 are interchanged, and the apparent size difference is

$$\Delta^* = \eta_1 R_1 - R_2. \tag{27}$$

Consequently, Eq. (23) becomes

$$a = \left[a_2^3 + 3(1-x)\frac{\gamma}{\gamma_2}a_2^2(\zeta a_1 - a_2)\right]^{1/3}, \qquad \frac{\gamma}{\gamma_2} = \frac{1 + 4\mu_2/3\kappa}{1 + 4\mu_2/3\kappa_1}, \tag{28}$$

where

$$\zeta = \eta_1\sqrt[3]{\frac{\vartheta_1 k_2}{\vartheta_2 k_1}}. \tag{29}$$

For nearly equal atomic volumes of the solute and solvent, the lattice parameter becomes

$$a = \left[\zeta\frac{\gamma}{\gamma_2}(1-x)\right]a_1 + \left[1 - \frac{\gamma}{\gamma_2}(1-x)\right]a_2. \tag{30}$$

Neither of the derived equations (25) or (30) is in agreement with a simple linear dependence between the effective lattice parameter and the solute concentration,

$$a^{\mathrm{V}} = (1-x)a_1 + xa_2. \tag{31}$$

This empirical relationship was observed in an early application of the X-rays diffraction to study the crystalline structure by Vegard (1921), who noticed that it approximately holds for many mutually soluble pairs of ionic salts at constant temperature. The observation has become known as Vegard's law or rule, although, when subsequently applied to other solid solutions, particularly metallic alloys, the law was found to be seldomly obeyed (Hume-Rothery et al., 1969; Pearson, 1972). By comparing Eq. (25) with Eq. (31), a deviation from the Vegard's law is

$$a - a^{\mathrm{V}} = \left[\left(1 - \frac{\gamma}{\gamma_2}\right)a_1 - \left(1 - \zeta\frac{\gamma}{\gamma_2}\right)a_2\right]x. \tag{32}$$

This is equal to zero only if $\zeta = 1$ and $\gamma = \gamma_2$, i.e., if the solute and solvent share the same crystalline structure (isostructural elements), if the apparent radius of the solute is taken to be the radius of the solute in its home environment, and if the elastic properties of the solute and solvent are identical. As an illustration, for two isostructural elements with different elastic properties, positive deviation from Vegard's law ($a > a^{\mathrm{V}}$) occurs when $(\kappa - \kappa_2)(a_1 - a_2) > 0$. Thus, if the solute is more compressible than the solvent, positive deviation occurs if the solute atom is smaller than the solvent atom. Pines (1940) suggested that elements with larger atoms tend to be more compressible, and, consequently, the negative sign of deviation from Vegard's law is met more often than the positive sign. For many systems the sign of deviation is not constant along the composition. Friedel (1955) calculated deviations from Vegard's law resulting from the difference in compressibilities of the solute and solvent for a number of solid solutions. Although in some alloy systems the agreement was good, for alloys of copper, silver and gold with each other, deviations were very different from the observed values (see, e.g., Table 1 of Mott, 1962). King (1966) indicated that in alloys where the solute atom is smaller than the solvent, the sign of the predicted change in atomic volume was always wrong. Where the atomic volume of the solute is greater, the predicted and observed values agreed to within 5% in only half of the considered random selection of alloy systems. In the case of Cu–Ag and Cu–Au alloys, deviations were opposite in sign to observed deviations. The results for solutions based on iron, aluminum and magnesium were also poor. For Au–Ag alloy, both the

Vegard's law and Eq. (25), with $\zeta = 1$, predict an increase of the effective lattice parameter due to substitution of larger silver atom in the solvent matrix of smaller gold atoms. Precise measurements, however, indicate a decrease of the effective lattice parameter (see Table 2 of King, 1966, or Tables 4–10 of Pearson, 1972). The size effect by itself cannot explain such behavior. Similar situation is found in other systems. The lattice distortion of the nickel lattice with germanium as the solute is opposite in sense to that expected from the relative sizes of the elemental atoms. Considering the latter case, Chessin et al. (1963) proposed a model in which the atom is regarded to consist of a hard incompressible core, surrounded by a compressible shell, smeared out through the space not filled by the hard cores (e.g., 0.26 of the unit cell volume in FCC, and 0.32 in BCC structure).

7. Results based on the apparent radius of solute atom

Lattice parameters and atomic radii of selected elements at room temperature are listed in Table 1. In the absence of theory which can predict the apparent radius of the solute atom in solvent environment solely in terms of the atomic properties of pure solute and solvent, the apparent radius of the solute atom will be estimated by using one experimental information about the solid solution, i.e., the initial slope of the lattice spacing vs. composition curve, $(\mathrm{d}a/\mathrm{d}x)_{x=0}$. This is related to the volume size factor ω_2 of King (1965) by

$$\omega_2 = \frac{1}{\Omega_1}\left(\frac{\mathrm{d}\Omega}{\mathrm{d}x}\right)_{x=0} = \frac{3}{a_1}\left(\frac{\mathrm{d}a}{\mathrm{d}x}\right)_{x=0}. \tag{33}$$

Numerical values of ω_2 for 469 metallic solid solutions, based on the precision lattice parameter data available in the literature, were listed by King (1966), and are reproduced for alloy systems considered in this paper in Table 2. By differentiation with respect to concentration x, from Eq. (18) we find that $\Omega_1\omega_2 = 4\pi R_1^3\gamma_1 C$. In the case of linear elasticity, the constant C is equal to $(R_2^* - R_1)/R_1\gamma_2$, and the apparent radius of the solute atom can be calculated from

Table 1
Lattice parameters and atomic radii (in units of Å) for selected elements at room temperature[a]

Element	Lattice	a c	$R_{\mathrm{c.d.}}$	R_{G}	R_{S}
Mg	HCP	3.2094	1.6047	1.6016	1.7703
		5.2107	(1.5985)		
Al	FCC	4.0496	1.4317	1.4317	1.5826
Si	DC	5.4306	1.1758	1.3361	1.6844
Ti	HCP	2.9506	1.4753	1.4616	1.6153
		4.6835	(1.4479)		
V	BCC	3.0240	1.3094	1.3499	1.4889
Cr	BCC	2.8850	1.2492	1.2878	1.4205
Mn	cubic	8.9140	1.1200	–	1.4286
Fe	BCC	2.8665	1.2412	1.2796	1.4114
Co	HCP	2.5071	1.2535	1.2510	1.3827
		4.0686	(1.2484)		
Ni	FCC	3.5240	1.2459	1.2459	1.3772
Cu	FCC	3.6146	1.2780	1.2780	1.4126
Zn	HCP	2.6648	1.3324	1.3944	1.5371
		4.9470	(1.4565)		
Ge	DC	5.6574	1.2250	1.3920	1.7548
Zr	HCP	3.2316	1.6158	1.6026	1.7713
		5.1475	(1.5894)		
Nb	BCC	3.2986	1.4283	1.4725	1.6219
Mo	BCC	3.1470	1.3627	1.4048	1.5495
Ag	FCC	4.0857	1.4445	1.4445	1.5969
Sn	cubic	6.4892	1.4050	–	1.8685
Ta	BCC	3.3030	1.4302	1.4744	1.6263
W	BCC	3.1652	1.3706	1.4130	1.5585
Au	FCC	4.0784	1.4420	1.4420	1.5939
Pb	FCC	4.9502	1.7502	1.7502	1.9345

[a] For FCC crystals the closest distance atomic radius is $R_{\mathrm{c.d.}} = a\sqrt{2}/4$, which is also equal to the Goldschmidt (C.N.12) radius R_{G}. For BCC crystals $R_{\mathrm{c.d.}} = a\sqrt{3}/4$, which is 3% less than R_{G}. For DC lattice $R_{\mathrm{c.d.}} = a\sqrt{3}/8$, 12% less than the corresponding R_{G}. For HCP (C.N.6,6) crystal $R_{\mathrm{c.d.}}$ is equal to $a/2$ or $\sqrt{a^2/3 + c^2/4}/2$, while R_{G} is taken to be the arithmetic mean of these two values. The Seitz radius R_{S} is calculated from the atomic volume, as explained in the text.

$$R_2^* = R_1\left(1 + \frac{\gamma_2}{3\gamma_1}\omega_2\right). \tag{34}$$

An analogous expression is derived for R_1^*. If a nonlinear elasticity is used, the constant C is given by Eq. (2), in which Δ is replaced by Δ^*. The apparent radius is then obtained by solving the resulting quadratic equation for R_2^*. In view of the uncertainties about the magnitudes of the third-order elastic constants for most metals (Landolt-Börnstein, 1979; Lubarda, 1997, 1999), the results based on the linear elasticity will only be pre-

Table 2
The volume size factor data: ω_1 is the volume size factor when the first element of the alloy system is the solute, and ω_2 when the second element is the solute

Alloy	ω_1	ω_2
Al–Ag	−0.0918	+0.0012
Al–Cu	+0.2000	−0.3780
Al–Mg	−0.3580	+0.4082
Al–Mn	+0.1620	−0.4681
Al–Ti	−0.2009	−0.1506
Al–Zn	−0.0625	−0.0574
Cu–Ag	−0.2775	+0.4352
Cu–Au	−0.2781	+0.4759
Cu–Fe	+0.1753	+0.0457
Cu–Ni	+0.0718	−0.0845
Cu–Zn	−0.5457	+0.1710
Fe–Co	+0.0524	+0.0154
Fe–V	−0.1886	+0.1051
Ag–Au	−0.0064	−0.0178
Ag–Mg	−0.6342	+0.0713
Si–Ge	−0.2065	+0.0468
Nb–Ta	−0.0023	−0.0026
Pb–Sn	+0.2905	−0.0825
Ti–Zr	−0.2233	+0.3008
Cr–W	−0.2173	+0.3735

Table 3
Elastic constants for polycrystalline metals[a]

Element	κ (GPa)	μ (GPa)
Mg	35.6	17.3
Al	72.6	26.0
Si	97.6	66.2
Ti	108.2	45.6
V	157.9	46.7
Cr	160.0	115.1
Mn	98.0	39.0
Fe	169.6	81.4
Co	82.3	88.8
Ni	183	80.0
Cu	136.4	46.8
Zn	69.6	41.9
Ge	75.0	54.9
Zr	94.0	30.0
Nb	170.3	37.5
Mo	261.3	125.5
Ag	103.4	30.3
Sn	58.2	18.4
Ta	196.5	69.0
W	311.0	160.6
Au	170.7	27.5
Pb	45.9	5.6

[a] For Si, Ge, Au, W, Zr, Co, and Mn the constants are calculated from the single crystal constants by using the self-consistent method.

sented. The isotropic second-order elastic moduli used in calculations are recorded in Table 3. The values of the apparent radius obtained from Eq. (34), in the case of 20 considered alloy systems, are listed in Table 4. A detailed analysis of selected alloy combinations is as follows.

7.1. Al–Cu

The equilibrium diagram for this alloy is extremely complex between 30 and 50 at.% Al (Hansen and Anderko, 1958). Maximum solid solubility of copper in aluminum is about 2.5 at.% at 550 °C. This structure can be retained at room temperature by rapid quenching (supersaturated α_{Al} solution). Beyond this concentration, up to about 33 at.% (54 wt.%) of copper, the alloy is $(\alpha_{Al} + \theta)$ two phase mixture. The θ phase is an intermetallic compound Al_2Cu (b.c. tetragonal, C-16 type structure), which provides dispersion strengthening. At the opposite end of the phase diagram, aluminum is soluble in copper to about 20 at.% (α_{Cu} phase). Additional phases occur in-between, such as η_2, ζ_2 and δ (Al_2Cu_3) phase. The shear and bulk modulus of aluminum are assumed to be those of an isotropic polycrystalline aggregate, i.e., 26 and 72.6 GPa (Table 3). The corresponding values for copper are 46.8 and 136.4 GPa. The lattice parameter of aluminum at room temperature is 4.0496 Å, and of copper 3.6146 Å (Table 1; data from Barrett and Massalski, 1966, and Massalski et al., 1990). The Seitz radius of the aluminum atom in its parent crystalline structure is $R_1 = 1.5826$ Å, and of the copper is $R_2 = 1.4126$ Å. The apparent atomic radius of aluminum in copper lattice is $R_1^* = 1.5327$ Å. This is obtained by using the volume size factor $\omega_1 = 0.2$ from Table 2. The apparent radius of the copper in aluminum lattice is $R_2^* = 1.4133$ Å (Table 4). Solid curve in Fig. 1 shows the effective lattice parameter calculated from Eqs. (23) and (28). Eq. (23) was applied for the concentration range below $x = 0.5$, and Eq. (28) above, which gives a jump in the value of the effective lattice parameter at the midpoint of the concentration range. The experimental data for the two terminal solid solutions is indicated by

Table 4
Atomic radii of the elements in their parent lattices (R_1, R_2), and apparent atomic radii ($R_1^* = \eta_1 R_1$, $R_2^* = \eta_2 R_2$) of the solutes for selected alloy systems[a]

Alloy	R_1	R_2	η_1	η_2	R_1^*	R_2^*
Al–Ag	1.5826	1.5969	0.9745	0.9914	1.5422	1.5831
Al–Cu	1.5826	1.4126	0.9685	1.0005	1.5327	1.4133
Al–Mg	1.5826	1.7703	1.0565	1.0119	1.6015	1.8703
Al–Mn	1.5826	1.4286	0.9573	0.9494	1.5151	1.3563
Al–Ti	1.5826	1.6153	0.9403	0.9358	1.4881	1.5116
Al–Zn	1.5826	1.5371	0.9514	1.0096	1.5056	1.5519
Cu–Ag	1.4126	1.5969	1.0330	1.0258	1.4592	1.6380
Cu–Au	1.4126	1.5939	1.0191	1.0180	1.4396	1.6225
Cu–Fe	1.4126	1.4114	1.0627	1.0152	1.5011	1.4329
Cu–Ni	1.4126	1.3772	1.0010	0.9990	1.4140	1.3758
Cu–Zn	1.4126	1.5371	0.9333	0.9871	1.3184	1.5173
Fe–Co	1.4114	1.3827	0.9916	1.0281	1.3995	1.4216
Fe–V	1.4114	1.4889	0.9899	0.9821	1.3972	1.4623
Ag–Au	1.5969	1.5939	0.9958	0.9966	1.5901	1.5884
Ag–Mg	1.5969	1.7703	0.9349	0.9347	1.4927	1.6551
Si–Ge	1.6844	1.7548	0.9783	0.9770	1.6478	1.7145
Nb–Ta	1.6219	1.6263	1.0019	0.9964	1.6250	1.6205
Pb–Sn	1.9345	1.8685	1.0669	1.0077	2.0639	1.8829
Ti–Zr	1.6153	1.7713	1.0181	1.0084	1.6446	1.7861
Cr–W	1.4205	1.5585	0.9871	0.9980	1.4021	1.5553

[a] The radii are in the units of Å.

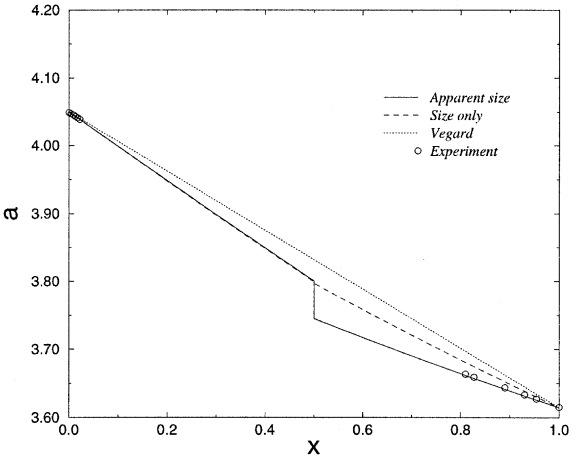

Fig. 1. Lattice parameter a (in Å) vs. concentration x for Al–Cu alloy system.The solid curve corresponds to continuum elasticity model with incorporated apparent size of the solute atom. Dashed curve is the same without incorporation of the apparent size, while dotted line is the effective lattice parameter according to Vegard's law. Experimental values for two terminal solid solutions are indicated by circles.

superimposed circles. These are taken from Pearson (1958, pp. 328 and 331). Good agreement between the calculations and experiment is evident at both ends of the concentration range. A dashed curve corresponds to the elasticity model which does not take into account the apparent size of the solute atom. A dotted line is a variation of the effective lattice parameter according to Vegard's law. Both latter predictions largely overestimate the effective lattice parameter of Cu-rich alloy.

7.2. Al–Ag

Maximum solid solubility of silver in aluminum is about 20 at.% Ag, at the eutectic temperature (566 °C). Maximum solid solubility of aluminum in silver is about 20 at.% Al, and occurs over wider range of temperature (Hansen and Anderko, 1958). The lattice spacing of Al based solution remains practically unchanged up to 6 at.% Ag; between 6 and 14 at.% there is an almost linear increase in spacing, while further additions up to about 27 at.% Ag cause little change in lattice parameter (see Fig. 62, p. 351 of Pearson, 1958). The lattice parameter of Ag based solution is basically linear with concentration up to about 10 at.% Al (Fig. 47, p. 263 of Pearson, 1958). The elasticity theory, without modification due to ap-

parent radius of the solute atom, predicts the effective lattice parameter in close agreement with Vegard's law, far overestimating the true lattice spacing. The incorporation of the apparent size (solid curve in Fig. 2) results in good agreement with experimental data at both ends of the concentration range. For example, from Table 5 it is seen that in the case of Al based solution the apparent misfit between the solute and solvent atom is practically equal to zero, while the original misfit, based on the sizes of two atoms in their parent lattices, is 0.014 Å.

7.3. Al–Mg

For this alloy system, Fig. 3 indicates that according to Vegard's law the lattice spacing of Al based alloy decreases with introduction of Mg solute atoms, while the observed behavior is opposite, i.e., the effective lattice parameter increases by introduction of (larger) Mg atoms. Superimposed circles are the measured values, taken from pp. 351 and 728 of Pearson, 1958. Similar remarks apply for Mg-rich solution, where the effective lattice spacing decreases with introduction of Al solute, in contrast to Vegard's law which predicts an increase of the effective lattice parameter. Therefore, for this alloy system there is a positive deviation from Vegard's law in Al-rich alloy, and negative deviation in Mg-rich alloy. Maximum solid solubility of magnesium in aluminum is about 18 at.% of Mg at 450 °C, and of aluminum in magnesium about 12 at.% of Al at 437 °C.

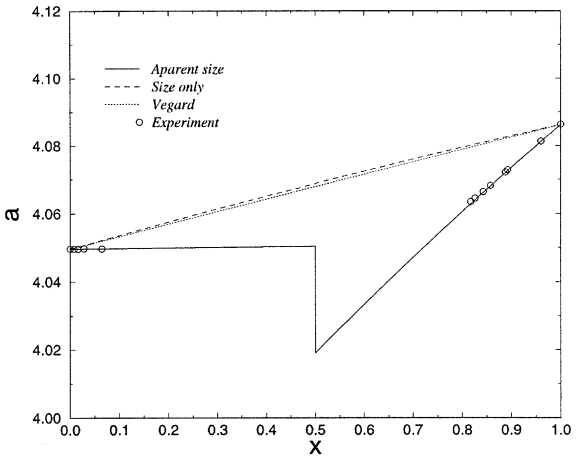

Fig. 2. Lattice parameter a (in Å) vs. concentration x for Al–Ag alloy system.

Table 5
Original and apparent misfits of atoms for selected alloy systems (in units of Å)

Alloy	$R_1 - R_2$	$R_1^* - R_2$	$R_1 - R_2^*$
Al–Ag	−0.0143	−0.0547	−0.0006
Al–Cu	+0.1700	+0.1201	+0.1693
Al–Mg	−0.1878	−0.1689	−0.2877
Al–Mn	+0.1540	+0.0865	+0.2262
Al–Ti	−0.0328	−0.1273	+0.0710
Al–Zn	+0.0455	−0.0314	+0.0307
Cu–Ag	−0.1843	−0.1377	−0.2254
Cu–Au	−0.1813	−0.1543	−0.2100
Cu–Fe	+0.0012	+0.0897	−0.0203
Cu–Ni	+0.0354	+0.0369	+0.0368
Cu–Zn	−0.1245	−0.2187	−0.1047
Fe–Co	+0.0287	+0.0168	−0.0102
Fe–V	−0.0775	−0.0918	−0.0509
Ag–Au	+0.0030	−0.0038	+0.0084
Ag–Mg	−0.1735	−0.2777	−0.0583
Si–Ge	−0.0703	−0.1070	−0.0300
Nb–Ta	−0.0044	−0.0013	+0.0014
Pb–Sn	+0.0660	+0.1953	+0.0516
Ti–Zr	−0.1559	−0.1267	−0.1708
Cr–W	−0.1380	−0.1563	−0.1348

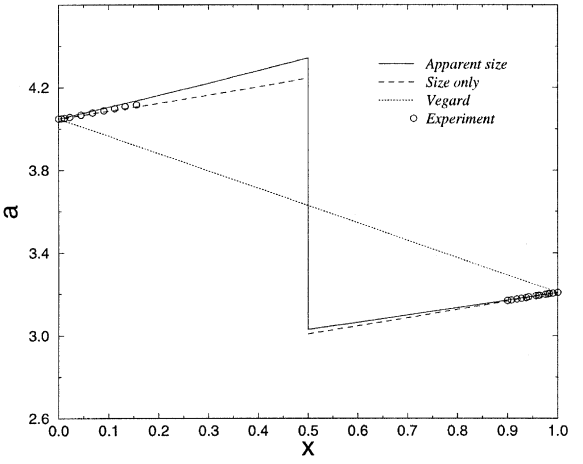

Fig. 3. Lattice parameter a (in Å) vs. concentration x for Al–Mg alloy system.

7.4. Cu–Au

Copper and gold form a continuous solid solution at high temperatures, while at lower

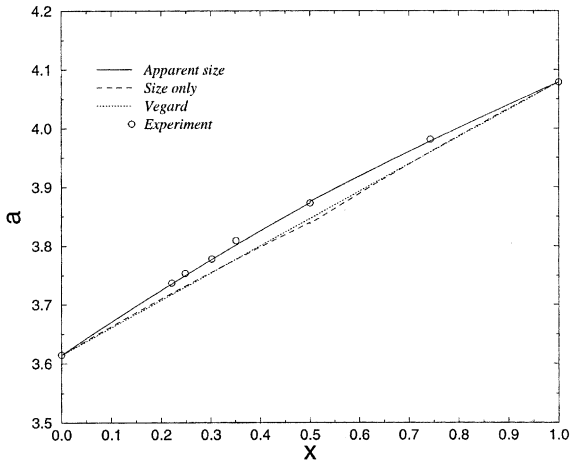

Fig. 4. Lattice parameter a (in Å) vs. concentration x for Cu–Au alloy system.

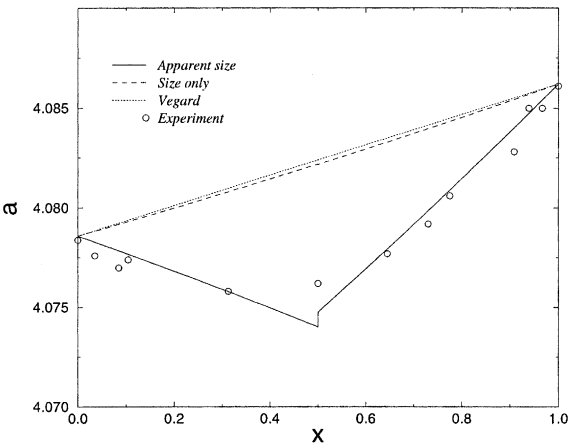

Fig. 5. Lattice parameter a (in Å) vs. concentration x for Au–Ag alloy system.

temperatures superlattices are formed about CuAu, Cu_3Au, and possibly $CuAu_3$. The circles in Fig. 4 correspond to measured values of the effective lattice parameter in quenched alloys, reported by Pearson (1958, pp. 411 and 601). Positive deviation from Vegard's law persists throughout the concentration range.

7.5. Ag–Au

Silver and gold form continuous series of solid solutions without formation of (superlattice) ordered structures at temperatures between the solidus and room temperature, although there is an indication for a partial, short-range ordering in the 50 at.% alloy. Fig. 5 shows the variation of the lattice parameter. Experimental data is from Pearson (1958, pp. 267 and 289). Negative deviation from Vegard's law persists throughout the concentration range. A notable feature of this alloy system is that the introduction of larger solute atoms of silver ($R_1 = 1.5969$ Å) in the solvent matrix of smaller gold atoms ($R_2 = 1.5939$ Å) actually decreases the volume and the effective lattice parameter of the resulting alloy. This is a consequence of the electronic interactions between the outer electron shells of the solute atom of silver and surrounding solvent atoms of gold, which shrinks the silver atom and makes it smaller than the gold atoms. Indeed, from Table 4 the apparent radius of silver atom in the gold matrix is $R_1^* = 1.5901$ Å, which is smaller than R_2. It should be, however, pointed out that the silver an gold atoms in their parent lattices are nearly equal in size, and that very precise measurements of the effective lattice parameter are needed to accurately record its variation with the solute concentration.

8. Free energy of binary alloys

The strain energy of a binary solid solution due to solute atoms resolved in the solvent matrix gives a significant contribution to the energy or heat of the formation of an alloy, which determines the degree to which two metals tend to alloy and is directly related to the structure of the corresponding phase diagrams. For a completely random (totally disordered) distribution of solutes, the configurational entropy is $-KN_1[x\ln x + (1-x)\ln(1-x)]$, where K is the Boltzmann constant. It is assumed that the number xN_1 is large enough for Sterling's approximation to be valid in the statistical derivation of the entropy expression. The free energy of formation of a binary alloy is then approximately

$$F = E + KN_1T[x\ln x + (1-x)\ln(1-x)], \qquad (35)$$

where T is the absolute temperature, and E is the strain energy. A general expression for the latter

can be deduced from the results obtained by Lubarda and Richmond (1999). For example, in the case of small misfit the strain energy is

$$E = N_1 E_0 x\left(1 - \frac{\gamma_1}{\gamma_2}x\right). \tag{36}$$

The self-energy of a single inserted solute atom is

$$E_0 = 6V_1\frac{\mu_1}{\gamma_2}\left(\frac{\Delta}{R_1}\right)^2, \quad V_1 = \frac{4}{3}R_1^3\pi. \tag{37}$$

The electro-chemical contribution to internal energy due to charge transfer, which lowers the energy of an alloy (e.g., Varley, 1954; Girifalco and Alonso, 1980), is not included in Eq. (35). Also neglected is a mixing entropy contribution due to the change in atomic vibrations around inserted solute atoms. The gradient of the specific free energy F/N_1 with respect to the concentration x is the corresponding thermodynamic force (affinity)

$$X = 6V_1\frac{\mu_1}{\gamma_2}\left(1 - 2\frac{\gamma_1}{\gamma_2}x\right)\left(\frac{\Delta}{R_1}\right)^2 - KT\ln\frac{1-x}{x}. \tag{38}$$

The first term represents an increase of the strain energy produced by insertion of an additional atom in the existing solution of concentration x. The last term is dominant at small x indicating a strong tendency for mixing of pure solvent in contact with another substance. The location of a possible spinode (inflection point) of the free energy is determined from the condition of the vanishing rate of X with respect to x, which gives

$$\frac{KT}{x(1-x)} = -12V_1\frac{\mu_1\gamma_1}{\gamma_2^2}\left(\frac{\Delta}{R_1}\right)^2. \tag{39}$$

The critical temperature T_g below which there is a miscibility gap in the phase diagram is obtained by requiring that a spinode point coincides with a minimum of the free energy curve. Thus, in addition to Eq. (39), the affinity vanishes in Eq. (38). The complete analysis requires the consideration of the free energy for other terminal solution, as well, particularly when this has a different crystalline structure.

In the case of small misfit with the elastic properties of the solute and solvent alike, the strain energy is $E/N_1 = E_0 x(1-x)$. Assuming this to apply throughout the concentration range, the corresponding free energy curve is concave downward, having the minimum at $x = 0.5$ for all temperatures greater than $T_g = E_0/2K$, which is in agreement with the prediction based on a quasi-chemical model of regular solutions (Swalin, 1972). The solute and solvent components will therefore have a temperature range of complete miscibility if T_g is lower than the lowest temperature on the solidus curve in the alloy's phase diagram. Friedel (1955) used this analysis to determine the limiting value of the size factor in binary alloys, and to deduce the Hume-Rothery 15% rule (Hume-Rothery et al., 1969).

The presented analysis applies to terminal solid solutions, or solid solutions with an unlimited solubility of two elements and one alloy phase throughout the concentration range. For most solutions, however, there is a range of concentration in which the free energy is lowered by ordering of solute atoms into appropriate aggregates. In this case there is a competition between a decrease of the strain energy due to clustering, and an increase of the free energy due to decrease of the configurational entropy, associated with the lost of complete randomness. The clustering zones appear to be spherical for very small misfits, and thin plate-like for large misfits (e.g., disk-shaped Guinier–Preston zones within (1 0 0) crystallographic planes in cubic crystals). There are alloys that show complete solid solubility at high temperature, whose solute atoms upon cooling organize in definite long-range order, superlattice structures. For instance, a disordered equiatomic alloy of copper and gold upon cooling takes a superlattice structure with alternate (1 0 0) planes occupied by copper and gold atoms. During formation of a superlattice in the solution of aluminum in iron, the aluminum atoms segregate to cube centers, avoiding the cubes that are side by side (avoiding to be nearest neighbors). In some alloy phases, an ordered structure is made by a particular (triangular or rectangular) ordering in close-packed crystallographic planes. Large difference in atomic size increases a tendency for ordering, since this relaxes the lattice strain of random solution. In addition, large and small atoms tend to group in

order to achieve more efficient packing (size factor phases). Interstitial type phases may form and these often have very complex structures (Laves phases). The alloy may also change its structure to avoid an undue increase in its electronic energy (electron compounds).

9. Discussion

The most important extension of the present work is to provide a theoretical basis for the analytical determination of the apparent radius of the solute atom in terms of the atomic properties of alloying elements in their pure state. This will require considerations from metal physics and physical chemistry. Separate consideration of various combinations of alloying elements may be needed, depending on their position in the periodic table and their electro-chemical characteristics. Wide solid solubility of one metal in another is in general favored by similar atomic sizes and equal valences of two elements, albeit these are not sufficient conditions for solid solubility. If atomic sizes and electronegativities are about the same, a metal of lower valence usually dissolves better one of higher valence than vice versa. The importance of various effects should be viewed having in mind that the metallic radius, valence and electronegativity are not truly independent quantities, since they all depend on the electronic configuration of an element and can be related to each other, for example, by an equation of the Gordon–Thomas type (Gschneidner, 1980).

Another extension of the present work is to study the intermediate phases in the equilibrium phase diagram, since an unlimited solvability of two elements, and the existence of only one alloy phase throughout the concentration range has been assumed in the present work. There has been a significant amount of research devoted to cluster formation and interactions through atomistic calculations and first-principles approach (e.g., Takai et al., 1982; Gonis et al., 1989). A semi-empirical cellular model was also developed in a series of papers by Miedema and coworkers, which allows a determination of the heat of formation in intermetallic compounds (Miedema and Châtel, 1980). The nonlinear and nonlocal elasticity may prove to be a bridge between electronic/atomic models and continuum models. By adding nonlinearity and nonlocality in the vicinity of dilatation centers, some of the essential features from the nanoscale may be captured. For example, there has been a computationally intensive two-scale modeling in which the severely deformed regions are described by an atomistic scale model, while outer regions are modeled by a local linear elasticity (Tadmor et al., 1996; Phillips, 2001). With rapidly improving situation in computational quantum mechanics, the coefficients of nonlinearity and nonlocality could be computed from first principles, rather than being inferred from sensitive measurements. This will enable us to say more accurately, for example, what additions of copper or magnesium to an aluminum alloy should do to such quantities as lattice volume, dislocation mobility, grain boundary energy, etc.

Acknowledgements

This work has been motivated by a series of communications with the late Dr. Owen Richmond. His insight to mechanics and physics of solids has influenced my work over a number of years and is greatly appreciated. A research support from the Montenegrin Academy of Sciences and Arts is also acknowledged.

References

Axon, H.J., Hume-Rothery, W., 1948. The lattice spacings of solid solutions of different elements in aluminium. Proc. Roy. Soc. A 193, 1–24.

Barrett, C.S., Massalski, T.B., 1966. Structure of Metals, third ed McGraw-Hill, New York.

Blandin, A., 1965. Some applications of quantum mechanical calculations to the electronic structure of alloys. In: Massalski, T.B. (Ed.), Alloying Behavior and Effects in Concentrated Solid Solutions. Metall. Soc. Conf. 29, pp. 50–78.

Chessin, H., Arajs, S., Colvin, R.V., Miller, D.S., 1963. Paramagnetism and lattice parameters of iron-reach iron–germanium alloys. J. Phys. Chem. Solids 24, 261–273.

Eshelby, J.D., 1954. Distortion of a crystal by point imperfections. J. Appl. Phys. 25, 255–261.

Eshelby, J.D., 1956. The continuum theory of lattice deffects. Solid State Phys. 3, 79–144.

Finkler, D.K.-H., Maurer, A.E., Campbell, S.J., Heck, T., Gonser, U., 1987. Precision determination of the lattice parameters of CuAuFe alloys. Physica 145B, 335–341.

Friedel, J., 1954. Electronic structure of primary solid solutions in metals. Adv. Phys. 3, 446–507.

Friedel, J., 1955. Deviations from Vegard's law. Phil. Mag. 46, 514–516.

Ganguly, P., Shah, N., Phadke, M., Ramaswamy, V., Mulla, I.S., 1993. Deviation from Vegard's law: Changes in the *c*-axis parameter in $La_{2-x}Sr_xCuO_{4-d}$ in relation to the insulator–superconductor-metal transition. Phys. Rev. 47, 991–995.

Girifalco, L.A., Alonso, J.A., 1980. Energy-density approach to the theory of alloy formation. In: Bennett, L.H. (Ed.), Theory of Alloy Phase Formation. Metall. Soc. AIME, New York, pp. 218–261.

Gonis, A., Turchi, P.E.A., Zhang, X.-G., Stocks, G.M., Nicholson, D.M., Butler, W.H., 1989. Concentration dependent effective cluster interactions in substitutional alloys. In: Vitek, V., Srolovitz, D.J. (Eds.), Atomistic Simulations of Materials. Plenum Press, New York, pp. 15–28.

Gschneidner, K.A., Vineyard, G.H., 1962. Departures from Vegard's law. J. Appl. Phys. 33, 3444–3450.

Gschneidner, K.A., 1980. L.S. (Larry) Darken's contributions to the theory of alloy formation and where we are today. In: Bennett, L.H. (Ed.), Theory of Alloy Phase Formation. Metall. Soc. AIME, New York, pp. 1–39.

Hansen, M., Anderko, K., 1958. Constitution of Binary Alloys, second ed McGraw-Hill, New York.

Hume-Rothery, W., Smallman, R.E., Haworth, C.W., 1969. The Structure of Metals and Alloys. Institute of Metals, London.

King, H.W., 1965. Atomic volume and size correlations on solid solutions. In: Alloying Behavior and Effects in Concentrated Solid Solutions. In: Massalski, T.B. (Ed.), Metall. Soc. Conf., 29, pp. 85–104.

King, H.W., 1966. Quantitative size-factors for metallic solid solutions. J. Mater. Sci. 1, 79–90.

Landolt-Börnstein, 1979. Numerical Data and Functional Relationships in Science and Technology. In: Hellwege, K.-H., Hellwege, A.M. (Eds.), Group III, vol. 11. Springer-Verlag, Berlin (Also, vol. 2, 1969).

Lawson, A.W., 1947. On simple binary solid solutions. J. Chem Phys. 15, 831–842.

Lubarda, V.A., 1997. New estimates of the third-order elastic constants for isotropic aggregates of cubic crystals. J. Mech. Phys. Solids 45, 471–490.

Lubarda, V.A., 1999. Apparent elastic constants of cubic crystals and their pressure derivatives. Int. J. Nonlinear Mech. 34, 5–11.

Lubarda, V.A., Richmond, O., 1999. Second-order elastic analysis of dilute distribution of spherical inclusions. Mech. Mater. 31, 1–8.

Massalski, T.B., Subramanian, P.R., Okamoto, H., Kacprzak, L., 1990. Binary Alloy Phase Diagrams, second ed., vol. 1–3. Am. Soc. Metals Mater., Park, Ohio.

Massalski, T.B., King, H.W., 1961. Alloy phases of the noble metals. Prog. Mater. Sci. 10, 1–78.

Miedema, A.R., Châtel, P.F., 1980. A semi-empirical approach to the heat of formation problem. In: Bennett, L.H. (Ed.), Theory of Alloy Phase Formation. Metall. Soc. AIME, New York, pp. 344–389.

Mott, N.F., 1962. The cohesive forces in metals and alloys. Rep. Progr. Phys. 25, 218–243.

Murnaghan, F.D., 1951. Finite Deformation of an Elastic Solid. John-Wiley and Sons, New York.

Nemat-Nasser, S., Hori, M., 1999. Micromechanics: Overall Properties of Heterogeneous Materials (second revised ed.). Elsevier, Amsterdam.

Nongkynrih, P., Rao, Y.S.T., Gupta, S.K., Rao, P.V.R., 1988. Crystal structure of the substituted apatites – deviation from Vegard's law. J. Mater. Sci. 23, 3243–3247.

Park, M., Mitchell, T.E., Heuer, A.H., 1975. Subsolidus equilibria in the TiO_2–SnO_2 system. J. Am. Ceramic Soc. 58, 43–47.

Pauling, L., 1956. An electronic structure of metals and alloys. In: Theory of Alloy Phases. American Society for Metals, Cleveland, Ohio, pp. 220–242.

Pauling, W., 1960. The Nature of the Chemical Bond, third ed Cornell University Press, Ithaca, New York.

Pearson, W.B., 1958. In: Handbook of Lattice Spacings and Structures of Metals and Alloys, vol. 1. Pergamon Press, London.

Pearson, W.B., 1972. The Crystal Chemistry and Physics of Metals and Alloys. John Wiley, New York.

Phillips, R.B., 2001. Crystals, Defects and Microstructures: Modeling Across Scales. Cambridge University Press, Cambridge.

Pines, B.J., 1940. On solid solutions. J. Phys. 3, 309–319.

Sarkisov, E.S., 1960. Variation in the lattice constants of solid solutions with composition and Vegard's rule. Russian J. Phys. Chem. 34, 202–205.

Seeger, A., Mann, E., 1959. Anwendung der nichtlinearen Elastizitätstheorie auf Fehlstellen in Kristallen. Z. Naturforschg. 14a, 154–164.

Seitz, F., 1946. Color centers in alkali halide crystals. Rev. Mod. Phys. 18, 384–408.

Solin, S.A., Lee, S., Miyazaki, H., Mahanti, S.D., 1989. *C*-axis lattice expansion in ternary intercalated layered solids. Synt. Metals 34, 243–248.

Steinwehr, H.E.V., 1967. Ursachen der Abweichungen von der Vegardschen Regel. Z. Kristallogr. 125, 360–376.

Swalin, R.A., 1972. Thermodynamics of Solids. John Wiley, New York.

Tadmor, E.B., Ortiz, M., Phillips, R.B., 1996. Quasicontinuum analysis of defects in solids. Phil. Mag. A 73, 1529–1563.

Takai, O., Doyama, M., Hisamatsu, Y., 1982. Pseudopotential formulation of point interactions in metals. In: Takamura, J.-I., Doyama, M., Kiritani, M. (Eds.), Point Defects and

Defect Interactions in Metals. University of Tokyo Press and North-Holland, Amsterdam, pp. 109–112.

Talanov, V.M., 1983. On the conditions pertaining to the applicability of Vegard's rule in spinel solid solution. J. Solid State Chem. 48, 86–92.

Toupin, R.A., Bernstein, B., 1961. Sound waves in deformed perfectly elastic materials—acoustoelastic effect. J. Acoust. Soc. Am. 33, 216–225.

Urusov, V.S., 1992. A geometric model of deviations from Vegard rule. J. Solid State Chem. 98, 223–236.

Varley, J.H.O., 1954. The calculation of heats of formation of binary alloys. Phil. Mag. 45, 887–916.

Vegard, L., 1921. Die Konstitution der Mischkristallen und die Raumfüllung der Atome. Z. fur Physik 5, 17–26.

Weiss, R.J., 1990. Physics of Materials. Hemisphere Publ, New York.

Yashima, M., Ishizawa, N., Yoshimura, M., 1992. Application of an ion-packing model based on defect clusters to zirconia solid solutions: II. Applicability of Vegard's law. J. Am. Ceram. Soc. 75, 1550–1557.

Zen, E-an, 1956. Validity of "Vegard's law". Am. Mineralogist 41, 523–524.

Zener, C., 1942. Theory of lattice expansion introduced by cold-work. Trans. Am. Inst. Min. (Metall.) Engrs. 147, 361–368.